POLAR PROPERTIES AND HYSTERESIS LOOPS IN MULTILAYERED THIN FILMS FERROELECTRIC/VIRTUAL FERROELECTRIC

E.A. ELISEEV,[1,2] M.D. GLINCHUK,[2] A.N. MOROZOVSKA,[1] YA.V. YAKOVENKO[3]

[1]**V.E. Lashkaryov Institute of Semiconductor Physics, Nat. Acad. of Sci. of Ukraine**
(41, Nauky Ave., Kyiv 03028, Ukraine; e-mail: eugene.a.eliseev@gmail.com)

[2]**I.M. Frantsevich Institute for Problems of Materials Science, Nat. Acad. of Sci. of Ukraine**
(3, Krzhyzhanivskyi Str., Kyiv 03142, Ukraine)

[3]**Taras Shevchenko National University of Kyiv, Faculty of Physics**
(2, Academician Glushkov Ave., Bld. 1, Kyiv 03127, Ukraine)

PACS 77.80.B-, 77.55.fe

In the framework of Landau–Ginzburg–Devonshire (LGD) phenomenological theory, the influence of misfit strains, surface energy, and finite-size effects on phase diagrams, polar properties, and hysteresis loops has been calculated for multilayered thin films of the type ferroelectric/virtual ferroelectric. The influence of elastic deformations that arise at the interface thin film–substrate owing to a mismatch between the lattice constants in the film and the substrate on the phase diagrams of multilayered thin films virtual ferroelectric $SrTiO_3$/ferroelectric $BaTiO_3$ has been studied for the first time. In contrast to bulk $BaTiO_3$, in which only four phases (cubic, tetragonal, orthorhombic, and rhombohedral) can exist, it turned out that six thermodynamically stable $BaTiO_3$ phases (paraelectric phase and tetragonal (FEc), two monoclinic (FEaac and FEac), and two orthorhombic (FEa and FEaa) ferroelectric phases) can exist in multilayered $SrTiO_3/BaTiO_3$ films. The main polar properties of hysteresis loops (shape, coercive field, and spontaneous polarization) in thin multilayered $SrTiO_3/BaTiO_3$ films are calculated. It is shown that the system demonstrates a strong dependence of its polar properties on the thickness of $SrTiO_3$ and $BaTiO_3$ layers, as well as on the elastic misfit strains, with $SrTiO_3$ playing the role of dielectric layer: the thicker the layer, the stronger is the depolarization field, which, in its turn, reduces the spontaneous polarization in the $BaTiO_3$ film.

1. Introduction

Multilayer ferroelectric films are challenging objects for experimental and theoretical researches, because they demonstrate enhanced polar properties in comparison with monolayer films of the same thickness. However, the influence of misfit strains that arise owing to the difference between the elastic properties of the substrate and the multilayer film on the phase diagrams and the polar properties of and the hysteresis loops in multilayer thin films of the type ferroelectric/virtual ferroelectric has almost not been studied theoretically.

1.1. Current state of experimental researches dealing with the polar properties of multilayer ferroelectric films

Multilayer ferroelectric films and compositionally graded heterostructures demonstrate an enhanced spontaneous polarization, a huge pyroelectric response, and a large piezoelectric deformation (see, e.g., work [1] and the references therein). Electric and electromechanical properties of complicated oxide superfilms $CaTiO_3/BaTiO_3$ are closely connected with the structure evolution and the electric polarization in every layer induced by an applied electric field. The coexistence of elastic deformations and rotations of oxygen octahedra near the interface between polar and nonpolar film layers allows this system to show a rich spectrum of nanoscaled phenomena. Multilayer materials with improved functional characteristics are of interest for the development of nanophysics and nanotechnology. For instance, a piezoelectric response to an applied electric field arises in the $CaTiO_3$ dielectric layers of nano-sized multilayer dielectric-ferroelectric films $CaTiO_3/BaTiO_3$ [2, 3]. The measured piezoelectric coefficient of 54 pm/V agrees with the results of *ab initio* calculations, in which the tetragonal symmetry in the superfilm is supposed to be induced by the $SrTiO_3$ substrate.

Stephanovich *et al.* [4] studied the ferroelectric phase transition and the formation of domains in a periodic multilayer film consisting of alternating ferro- and paraelectric nano-sized layers. They found that ferroelectric domains formed in different ferroelectric layers

can interact with one another through the paraelectric layer. By minimizing the Ginzburg–Landau functional, those authors calculated the critical transition temperature T_c as a function of the thickness of a multilayer ferro-/paraelectric film. However, the influence of the strains arising owing to a misfit between the substrate and the multilayer film on the polar properties of the system was not studied.

The theoretical approach is considered to be necessary in the effective search for thin films and their multilayer structures with considerably improved functional properties [5]. The development and the application of methods aimed at growing the thin films of functional oxides are at the beginning, and plenty of obstacles should be overcome expectedly for a better structural monitoring of layer quantity to be developed, as well as for the reproducibility and the monitoring of the corresponding electrophysical, polar, optical, and spintronic properties to be achieved.

1.2. Current state of theoretical researches dealing with the polar properties of multilayer ferroelectric films

1.2.1. Theoretical calculations of polar properties of multilayer ferroelectric films

Ab initio calculations [6] of polar and piezoelectric properties of a $CaTiO_3/BaTiO_3$ superfilm grown up on a $SrTiO_3$ substrate showed that short-period superfilms have a higher spontaneous polarization than that of long-period ones. A thermodynamic model [7] for the polarization and the dielectric response of ferro-/paraelectric bilayers and multilayer films was proposed. The strong electrostatic coupling between the layers was shown to suppress the ferroelectric behavior at a critical thickness of the paraelectric layer. A bilayer is characterized by a giant dielectric response, which is similar to the dielectric anomaly in a vicinity of the Curie–Weiss temperature in a homogeneous ferroelectric with a critical thickness. The numerical analysis carried out for a pseudomorphic (001) heteroepitaxial $BaTiO_3/SrTiO_3$ bilayer on a (001) $SrTiO_3$ substrate and an undeformed $BaTiO_3/SrTiO_3$ bilayer showed that the polarization and the dielectric peak disappear totally at $SrTiO_3$ contents of about 66 and 14% in those two systems, respectively.

It was shown from the first principles that the ground state of a system consisting of a multilayer film of the type ferroelectric/paraelectric, $PbTiO_3/SrTiO_3$, is not purely ferroelectric. It also includes antiferrodistortive rotations of oxygen octahedra, which are an analog of nonintrinsic ferroelectricity. In addition, the dielectric response of the system was found to have a weak temperature dependence. The results obtained theoretically were demonstrated to agree with those of experimental observations [8].

Fong *et al.* [9] connected the critical character of the thickness of a thin ferroelectric film with the presence of a near-surface layer, which includes rotated oxygen octahedra reconstructed into a surface antiferrodistortive structure.

1.2.2. Theoretical calculations of polar properties of multilayer ferroelectric films in the framework of LGD phenomenological theory

Numerical calculations were carried out for heteroepitaxial (001) bilayers and (001) multilayer $PbTiO_3/SrTiO_3$ (PTO/STO) structures on (001) STO substrates. Similarly to the temperature dependence inherent to a homogeneous ferroelectric, there exists a critical value for the PTO layer, below which the bilayer or multilayer film is in the paraelectric state. This critical thickness depends strongly on the density of coupled charges at the interface between the films. The results of calculations for the dielectric response show that the ferroelectric phase transition, which is well-pronounced for uncharged bilayers and superfilms, gets smeared, and the total dielectric constant decreases, as the charge density increases [10, 11]. In works [10, 11], the nonlinear thermodynamic model was used to study the role of interfaces in the polarization response of a ferroelectric-paraelectric bilayer, and the numerical analysis was made for a BTO/STO bilayer. The critical thickness was predicted for $SrTiO_3$, at which the spontaneous polarization in $BaTiO_3$ should disappear owing to the growth of the depolarization field. The critical thickness was demonstrated to decrease together with a reduction of the total bilayer thickness, by indicating the fact that the interface effects are more pronounced in thinner bilayers [12].

The LGD formalism enables the ferroelectric properties of many materials to be described adequately. In most cases, only one phase characterized by the components of its polarization oriented in the film plane was revealed in thin films of ferroelectric perovskites (see, e.g., works [13–15]). In particular, the properties of phase transitions and mechanisms of domain structure formation in films consisting of alternating ferroelectric and paraelectric nano-sized layers were studied. The domain structure period and the temperatures of phase transitions were found to depend on the thickness of ferro- and paraelectric layers [4].

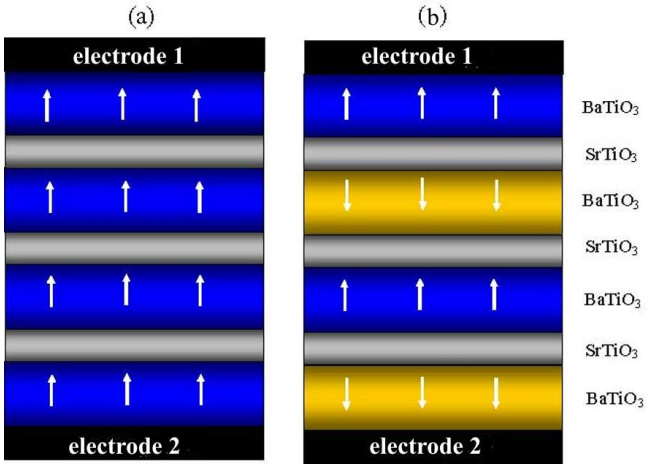

Fig. 1. Probable polarization configurations in a multilayered BTO/STO film

By analyzing the literature, it is possible to conclude that, up to now, the influence of misfit strains, which arise owing to the difference between the elastic properties of the substrate and the multilayer film, on the phase diagrams, polar properties, and hysteresis loops in multilayer thin films of the type ferroelectric/virtual ferroelectric has not been studied enough theoretically. Therefore, in what follows, we consider multilayer films consisting of films of different materials.

2. Mathematical Formulation of the Problem

This work is aimed at (i) calculating the influence of misfit strains, surface energy, and size effects (i.e. the dependence on the ratio between the layer thicknesses) on the phase diagrams, polar properties, and hysteresis loops in thin multilayer films of the type ferroelectric/virtual ferroelectric material and (ii) establishing the influence of elastic deformations that arise at the interface between the thin film and the substrate owing to a mismatch between their lattice constants on the phase diagrams of thin multilayer thin films virtual ferroelectric ($SrTiO_3$)/ferroelectric ($BaTiO_3$). Probable monodomain configurations of the polarization in a multilayer BTO/STO film are illustrated in Fig. 1.

Monodomain states of the system can be described analytically, because the corresponding problem is reduced to a one-dimensional one. Those states can be realized in the case of defect-free multilayer films sandwiched between two conducting electrodes. The monodomain state has a lower correlation energy and a lower energy of domain walls than the polydomain one has. For a film without electrodes (or with semiconductor electrodes), the polydomain state is energetically beneficial, because it has a lower depolarization field, although the energy of domain walls is higher. As is shown below, the monodomain state corresponds expectedly to solitary hysteresis loops of ferroelectric polarization.

The free energy functional for the multilayer system depicted in Fig. 1 includes the energy of every layer and the energies of interfaces,

$$F = F_{\text{layer}} + F_{\text{interface}}, \tag{1a}$$

$$F_{\text{layer}} = \sum_{i=1}^{n} \int_{z_{i-1}}^{z_i} \Delta F_b^{(i)} \left(P_1^{(i)}, P_2^{(i)}, P_3^{(i)} \right) dz, \tag{1b}$$

$$F_{\text{interface}} = \left(\begin{array}{c} \sum\limits_{i=1}^{n} \left(\left(\frac{\alpha_{i1}^{(i)}}{2} \left(P_1^{(i)} \right)^2 + \frac{\alpha_{i2}^{(i)}}{2} \left(P_2^{(i)} \right)^2 + \frac{\alpha_{i3}^{(i)}}{2} \left(P_3^{(i)} \right)^2 \right) \Big|_{z=z_{i-1}} + \right. \\ \left. + \left(\frac{\alpha_{r1}^{(i)}}{2} \left(P_1^{(i)} \right)^2 + \frac{\alpha_{r2}^{(i)}}{2} \left(P_2^{(i)} \right)^2 + \frac{\alpha_{r3}^{(i)}}{2} \left(P_3^{(i)} \right)^2 \right) \Big|_{z=z_i} \right) + \\ + \sum\limits_{i=1}^{n-1} \left(\frac{\gamma_1^{(i)}}{2} \left(P_1^{(i)} - P_1^{(i+1)} \right)^2 + \frac{\gamma_2^{(i)}}{2} \left(P_2^{(i)} - P_2^{(i+1)} \right)^2 + \frac{\gamma_3^{(i)}}{2} \left(P_3^{(i)} - P_3^{(i+1)} \right)^2 \right) \Big|_{z=z_i} \end{array} \right). \tag{1c}$$

Here, we introduced the following notation: h_i is the thickness of the i-th layer, and z_i is the position of interface between different layers, so that $z_i = \sum_{j=1}^{j=i} h_j$ and $z_0 = 0$. The surface energy (1c) is similar to that of a monolayer. The last term corresponds to the interaction between polarization components belonging to neighbor layers [16]. The expression for the surface energy includes only the terms, which are allowed by the tetragonal symmetry. The terms linear in $P_3^{(i)}$ are excluded, because they would result in a spontaneous

polarization of the nonpolar paraelectric phase. From the condition of polarization continuity, we adopt that $\alpha_{rj}^{(i)} = \alpha_{lj}^{(i+1)} = \gamma_j^{(i)}$ in Eq. (1c). The surface terms in Eq. (1c) have a meaning of the squared polarization gradient between layers (see work [17]); in particular, in the limiting case $\gamma_j^{(i)} \to \infty$, the polarization on the surface $P_j^{(i)} \equiv P_j^{(i+1)}$.

The density of the bulk part of the free energy ΔF_b for the paraelectric phase with initial symmetry $m3m$, which corresponds to the symmetry of every $BaTiO_3$ or $SrTiO_3$ layer, can be written down as a Taylor expansion in the polarization components P_k ($k = 1, 2, 3$):

$$\Delta F_b^{(i)}\left(P_1, P_2, P_3\right) = \left(\begin{array}{l} \frac{a_1^{(i)}}{2}\left(P_1^2+P_2^2\right)+\frac{a_3^{(i)}}{2}P_3^2+\frac{a_{12}^{(i)}}{2}P_1^2P_2^2+\frac{a_{13}^{(i)}}{2}P_3^2\left(P_2^2+P_1^2\right)+ \\ +\frac{a_{11}^{(i)}}{4}\left(P_1^4+P_2^4\right)+\frac{a_{33}^{(i)}}{4}P_3^4+\frac{a_{111}^{(i)}}{6}\left(P_1^6+P_2^6+P_3^6\right)+\frac{a_{123}^{(i)}}{2}P_3^2P_2^2P_1^2+ \\ +\frac{a_{112}^{(i)}}{4}\left(P_3^4\left(P_1^2+P_2^2\right)+P_1^4\left(P_2^2+P_3^2\right)+P_2^4\left(P_1^2+P_3^2\right)\right)+ \\ +\frac{g_{11}^{(i)}}{2}\left(\frac{\partial P_3}{\partial z}\right)^2+\frac{g_{44}^{(i)}}{2}\left(\left(\frac{\partial P_1}{\partial z}\right)^2+\left(\frac{\partial P_2}{\partial z}\right)^2\right)-\frac{1}{2}P_3E_3^{d(i)}-P_3E_3^e \end{array} \right). \quad (2)$$

Here, we used the Voigt notation and the Cartesian coordinates. The surface cross-section (100) is considered. The quantities g_{ij} are the gradient coefficients of the ferroelectric. We also take into account that the equilibrium state for the thin film on the substrate will be found as a minimum of the Helmholtz free energy $F = G_+ \int_V u_{jk} X_{jk} d^3r$, which can be obtained from the Hibbs free energy using the Legendre transformation [18].

The mismatch of the lattice constants between the film and the substrate causes a redefinition of the free energy coefficients due to the misfit strain $u_m^{(i)} = \frac{c_i - c_S}{c_S}$ that emerges between the multilayer film and the substrate,

$$a_1^{(i)} = 2\alpha_1^{(i)}(T) - \frac{2\left(Q_{11}^{(i)}+Q_{12}^{(i)}\right)}{s_{11}^{(i)}+s_{12}^{(i)}}u_m^{(i)},$$

$$a_3^{(i)} = 2\alpha_1^{(i)}(T) - \frac{4Q_{12}^{(i)}}{s_{11}^{(i)}+s_{12}^{(i)}}u_m^{(i)}, \quad (3a)$$

$$a_{11}^{(i)} = 4\alpha_{11}^{(i)} + 2\frac{\left(Q_{11}^{(i)2}+Q_{12}^{(i)2}\right)s_{11}^{(i)} - 2s_{12}^{(i)}Q_{11}^{(i)}Q_{12}^{(i)}}{s_{11}^{(i)2}-s_{12}^{(i)2}},$$

$$a_{33}^{(i)} = 4\alpha_{11}^{(i)} + \frac{4Q_{12}^{(i)2}}{s_{11}^{(i)}+s_{12}^{(i)}}, \quad (3b)$$

$$a_{12}^{(i)} = 2\alpha_{12}^{(i)} - 2\frac{\left(Q_{11}^{(i)2}+Q_{12}^{(i)2}\right)s_{12}^{(i)} - 2s_{11}^{(i)}Q_{11}^{(i)}Q_{12}^{(i)}}{s_{11}^{(i)2}-s_{12}^{(i)2}} + \frac{Q_{44}^{(i)2}}{s_{44}^{(i)}},$$

$$a_{13}^{(i)} = 2\alpha_{13}^{(i)} + \frac{2Q_{12}^{(i)}\left(Q_{11}^{(i)}+Q_{12}^{(i)}\right)}{s_{11}^{(i)}+s_{12}^{(i)}}. \quad (3c)$$

Here, $\alpha_i^{(i)}$ and $\alpha_{ij}^{(i)}$ are the dielectric rigidity and the rigidity coefficients of higher order at a constant pressure, s_{11} and s_{12} are the coefficients of elastic compliance, Q_{ij} is the electrostriction tensor, and u_m is the misfit strain between the film and the substrate. The influence of misfit dislocations stimulates a relaxation of misfit strains. This fact can be taken into account by redefining u_m (see, e.g., [19]).

The quantity E_3^e in Eq. (2) is the external field, and E_3^d is the depolarization field arising owing to an incomplete screening of the polarization by the environment, a non-uniform distribution of the polarization, and/or its disappearance at the surface. For a one-dimensional distribution, the quantity E_3^d has the form

$$E_3^{(i)} = \frac{1}{\varepsilon_0 \varepsilon_b^{(i)}}\left(\frac{\sum\limits_{i=1}^{n} h_i \Big/ \varepsilon_b^{(i)} \left\langle P_3^{(i)} \right\rangle}{\sum\limits_{i=1}^{n} h_i \Big/ \varepsilon_b^{(i)}} - P_3^{(i)}\right), \quad (4)$$

where $\varepsilon_b^{(i)}$ is the background dielectric permittivity of the i-th layer, which is not connected with the soft optical mode [20], and $\left\langle P_3^{(i)} \right\rangle = \frac{1}{h_i}\int_{z_i}^{z_i+h_i} P_3^{(i)} dz$ is the average polarization of the i-th layer.

Below, we consider a periodic multilayer film with the geometrical period consisting of two layers, h_1 and h_2. The polarization distribution over different superperiods

$h_1 + h_2$ is supposed to be the same, which is valid, if the coefficients in the surface energy are independent of the surface arrangement. In the case of a one-dimensional distribution, the expression for the depolarization field can be simplified as follows:

$$E_3^{(1)} = \frac{1}{\varepsilon_0 \varepsilon_b^{(1)}} \times$$

$$\times \left(\frac{\left\langle P_3^{(1)} \right\rangle h_1 \Big/ \varepsilon_b^{(1)} + \left\langle P_3^{(2)} \right\rangle h_2 \Big/ \varepsilon_b^{(2)}}{h_1 \Big/ \varepsilon_b^{(1)} + h_2 \Big/ \varepsilon_b^{(2)}} - P_3^{(1)} \right), \tag{5}$$

$$E_3^{(2)} = \frac{1}{\varepsilon_0 \varepsilon_b^{(2)}} \times$$

$$\times \left(\frac{\left\langle P_3^{(1)} \right\rangle h_1 \Big/ \varepsilon_b^{(1)} + \left\langle P_3^{(2)} \right\rangle h_2 \Big/ \varepsilon_b^{(2)}}{h_1 \Big/ \varepsilon_b^{(1)} + h_2 \Big/ \varepsilon_b^{(2)}} - P_3^{(2)} \right). \tag{6}$$

One can see that the normal component of the polarization in a layer affects the normal component of the polarization in the other layer by means of the internal electric field.

3. Coupled Equations

The variation of the free energy functional brings about the following system of nonlinear Euler–Lagrange equations with the corresponding boundary conditions:

$$\begin{cases} (a_3^{(i)} + a_{13}^{(i)} (P_2^{(i)})^2 + a_{13}^{(i)} (P_1^{(i)})^2) P_3^{(i)} + \\ + a_{33}^{(i)} (P_3^{(i)})^3 + f_3^{(i)} - g_{11}^{(i)} \frac{\partial^2}{\partial z^2} P_3^{(i)} = E_3^{(i)}, \\ \left(\alpha_{S3}^{(i)} P_3^{(i)} + \gamma_3^{(i-1)} (P_3^{(i)} - P_3^{(i-1)}) - \right. \\ \left. - g_{11}^{(i)} \frac{dP_3^{(i)}}{dz} \right) \Bigg|_{z=z_{i-1}} = 0, \\ \left(\alpha_{S3}^{(i)} P_3^{(i)} + \gamma_3^{(i)} (P_3^{(i)} - P_3^{(i+1)}) + \right. \\ \left. + g_{11}^{(i)} \frac{dP_3^{(i)}}{dz} \right) \Bigg|_{z=z_i} = 0. \end{cases} \tag{7a}$$

$$\begin{cases} (a_1^{(i)} + a_{12}^{(i)} (P_1^{(i)})^2 + a_{13}^{(i)} (P_3^{(i)})^2) P_2^{(i)} + \\ + a_{11}^{(i)} (P_2^{(i)})^3 + f_2^{(i)} - g_{44}^{(i)} \frac{\partial^2}{\partial z^2} P_2^{(i)} = 0, \\ \left(\alpha_{S2}^{(i)} P_2^{(i)} + \gamma_2^{(i-1)} (P_2^{(i)} - P_2^{(i-1)}) - \right. \\ \left. - g_{44}^{(i)} \frac{dP_2^{(i)}}{dz} \right) \Bigg|_{z=z_{i-1}} = 0, \\ \left(\alpha_{S2}^{(i)} P_2^{(i)} + \gamma_2^{(i)} (P_2^{(i)} - P_2^{(i+1)}) + \right. \\ \left. + g_{44}^{(i)} \frac{dP_2^{(i)}}{dz} \right) \Bigg|_{z=z_i} = 0. \end{cases} \tag{7b}$$

$$\begin{cases} (a_1^{(i)} + a_{12}^{(i)} (P_2^{(i)})^2 + a_{13}^{(i)} (P_3^{(i)})^2) P_1^{(i)} + \\ + a_{11}^{(i)} (P_1^{(i)})^3 + f_1^{(i)} - g_{44}^{(i)} \frac{\partial^2}{\partial z^2} P_1^{(i)} = 0, \\ \left(\alpha_{S1}^{(i)} P_1^{(i)} + \gamma_1^{(i-1)} (P_1^{(i)} - P_1^{(i-1)}) - \right. \\ \left. - g_{44}^{(i)} \frac{dP_1^{(i)}}{dz} \right) \Bigg|_{z=z_{i-1}} = 0, \\ \left(\alpha_{S1}^{(i)} P_1^{(i)} + \gamma_1^{(i)} (P_1^{(i)} - P_1^{(i+1)}) + \right. \\ \left. + g_{44}^{(i)} \frac{dP_1^{(i)}}{dz} \right) \Bigg|_{z=z_i} = 0. \end{cases} \tag{7c}$$

Equations (7) are valid for every layer designated by the index "(i)". The electric field $E_3^{(i)} = E_3^{d(i)} + E_3^e$. The extrapolation length $\lambda_i = g_{1i}/\alpha$ was introduced, and its experimental values fall within the interval $\lambda = 0.5 \div 50$ nm [21].

The function

$$f_i = a_{111} P_i^5 + a_{123} P_i P_j^2 P_k^2 +$$

$$+ a_{112} \left(P_i^3 \left(P_j^2 + P_k^2 \right) + P_i \left(P_j^4 + P_k^4 \right) / 2 \right),$$

where $i, j, k = 1, 2, 3$ and $i \neq j \neq k$, depends on the fifth power of the polarization and, therefore, can be omitted for ferroelectrics with a second-kind phase transition. It is evident that the interlayer coupling is possible by means of the depolarization field and the surface interaction.

In the case of multilayer periodic systems with identical coefficients in the free energy expansion ($\gamma_j^{(i-1)} =$

$\gamma_j^{(i)} \equiv \gamma_j$), one may expect that the polarizations inside layers with identical structures would also be identical. Bearing in mind this simplification, we can transform Eqs. (7) into the following systems of equations with the corresponding boundary conditions:

$$\begin{cases} (a_3^{(1)} + 2a_{13}^{(1)}(P_i^{(1)})^2)P_3^{(1)} + a_{33}^{(1)}(P_3^{(1)})^3 + \\ + f_3^{(1)} - g_{11}^{(1)}\frac{\partial^2}{\partial z^2}P_3^{(1)} = E_3^{(1)}, \\ P_3^{(1)}\Big|_{z=-h_1} = P_3^{(1)}\Big|_{z=0}, \\ \left(\gamma_3(P_3^{(1)} - P_3^{(2)}) + g_{11}^{(1)}\frac{dP_3^{(1)}}{dz}\right)\Big|_{z=0} = 0. \end{cases} \tag{8a}$$

$$\begin{cases} (a_1^{(1)} + a_{12}^{(1)}(P_i^{(1)})^2 + a_{13}^{(1)}(P_3^{(1)})^2)P_i^{(1)} + \\ + a_{11}^{(1)}(P_i^{(1)})^3 + f_2^{(1)} - g_{44}^{(1)}\frac{\partial^2}{\partial z^2}P_i^{(1)} = 0, \\ P_i^{(1)}\Big|_{z=-h_1} = P_i^{(1)}\Big|_{z=0}, \\ \left(\gamma_i(P_i^{(1)} - P_i^{(2)}) + g_{44}^{(1)}\frac{dP_i^{(1)}}{dz}\right)\Big|_{z=0} = 0. \end{cases} \tag{8b}$$

$$\begin{cases} (a_3^{(2)} + 2a_{13}^{(2)}(P_i^{(2)})^2)P_3^{(2)} + a_{33}^{(2)}(P_3^{(2)})^3 + \\ + f_3^{(2)} - g_{11}^{(2)}\frac{\partial^2}{\partial z^2}P_3^{(2)} = E_3^{(2)}, \\ P_3^{(2)}\Big|_{z=0} = P_3^{(2)}\Big|_{z=h_2}, \\ \left(\gamma_3(P_3^{(2)} - P_3^{(1)}) - g_{11}^{(2)}\frac{dP_3^{(2)}}{dz}\right)\Big|_{z=0} = 0. \end{cases} \tag{9a}$$

$$\begin{cases} (a_1^{(2)} + a_{12}^{(2)}(P_i^{(2)})^2 + a_{13}^{(2)}(P_3^{(2)})^2)P_i^{(2)} + \\ + a_{11}^{(2)}(P_i^{(2)})^3 + f_2^{(2)} - g_{44}^{(2)}\frac{\partial^2}{\partial z^2}P_i^{(2)} = 0, \\ P_i^{(2)}\Big|_{z=0} = P_i^{(2)}\Big|_{z=h_1}, \\ \left(\gamma_i(P_i^{(2)} - P_i^{(1)}) + g_{44}^{(2)}\frac{dP_i^{(2)}}{dz}\right)\Big|_{z=0} = 0. \end{cases} \tag{9b}$$

Equations (8) and (9) correspond to layers (1) and (2), respectively, of the film. The polarization components for those layers are as follows: the components $P_3^{(1)}$ and $P_3^{(2)}$ are not oriented in the film plane, whereas the components $(P_i^{(1)})^2 = (P_1^{(1)})^2 = (P_2^{(1)})^2$ and $(P_i^{(2)})^2 = (P_1^{(2)})^2 = (P_2^{(2)})^2$ do.

4. Results of Numerical Simulation in 1D Monodomain Case

Let us numerically examine the one-dimensional monodomain case where $(P_i^{(1)})^2 \equiv 0$ and $P_3^{(1,2)} \neq 0$, as is illustrated in Fig. 1,*a*. The material parameters for a multilayer BTO/STO film, which were used at the simulation, are quoted in Appendix.

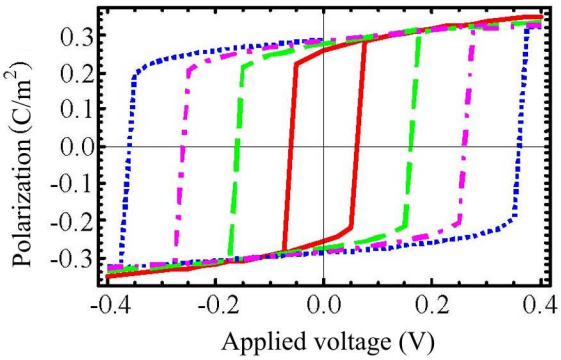

Fig. 2. Ferroelectric hysteresis loops in multilayer STO/BTO films with the thickness of BTO layer $h_{\rm BTO} = 5$ (solid), 9 (dashed), 13 (dah-dotted), and 17 (dotted curve) times the lattice constant. The STO layer thickness $h_{\rm STO} = 1$ lattice constant, the interface parameter $\gamma_3 = \gamma_i = 10^5$ C^{-2}m^{3}N, the misfit strain $u_m = -0.01$, the room temperature. Material parameters correspond to those of the multilayer BTO/STO film

The most important characteristic of the polarization switching in a multilayer film is the coercive field and the spontaneous polarization (see an example in Fig. 2). The corresponding dependences of the coercive field on the thickness of the virtual ferroelectric (STO) film calculated for various thicknesses of the ferroelectric (BTO) layer are depicted in Fig. 3,*a*. It is evident that the coercive field falls down as the thickness of STO film increases, so that STO plays a role of a dielectric layer: the thicker the layer, the stronger is the depolarization field (4), which, in its turn, depresses the ferroelectric properties of the BTO film. On the other hand, the coercive field increases with the BTO film thickness (cf. different curves).

The dependences of the coercive field on the BTO ferroelectric film thickness for various thicknesses of the STO layer are exhibited in Fig. 3,*b*. One can see that the coercive field monotonously grows with the BTO film thickness, which means that the thicker BTO layer possesses stronger ferroelectric properties. On the other hand, the coercive field diminishes, when the STO film thickness increases, and, as a result, the depolarization field grows (cf. different curves).

The corresponding dependences of the spontaneous polarization on the thickness of the STO virtual ferroelectric layer are shown in Fig. 4,*a* for various thicknesses of the BTO film. One can see that the spontaneous polarization monotonously decreases with the increase of the STO film thickness, so that STO plays the role of

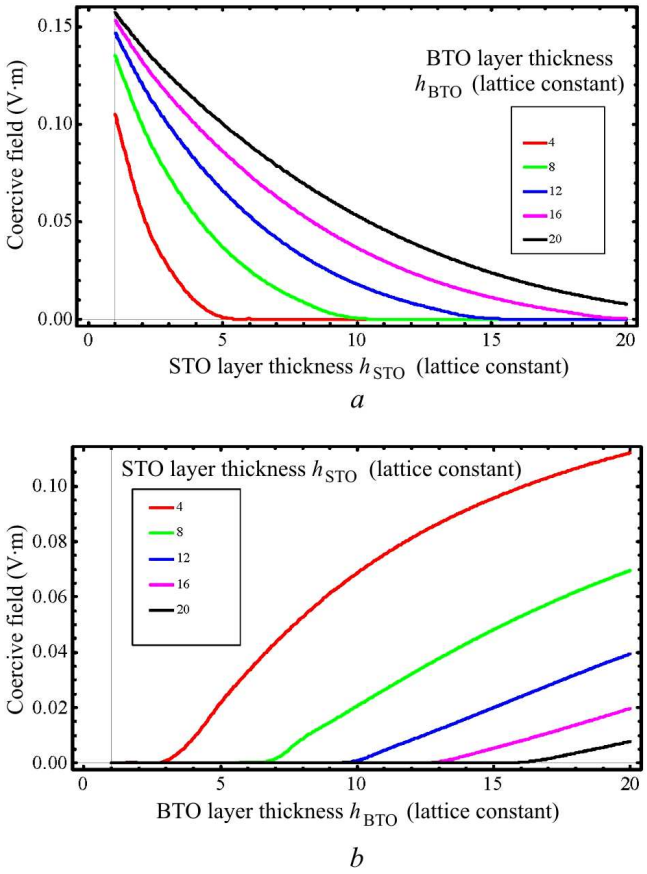

Fig. 3. (a) Dependences of the coercive field on the thickness h_{STO} of virtual ferroelectric STO layer for various thicknesses h_{BTO} of a ferroelectric BTO layer. (b) Dependences of the coercive field on the thickness h_{BTO} of a ferroelectric BTO layer for various thicknesses h_{STO} of the virtual ferroelectric STO layer. Both parameters are expressed in units of lattice constant. The interface parameter $\gamma_3 = \gamma_i = 10^5$ C^{-2}m^{3}N, the misfit strain $u_m = -0.01$, the room temperature. Material parameters correspond to those of the multilayer BTO/STO film

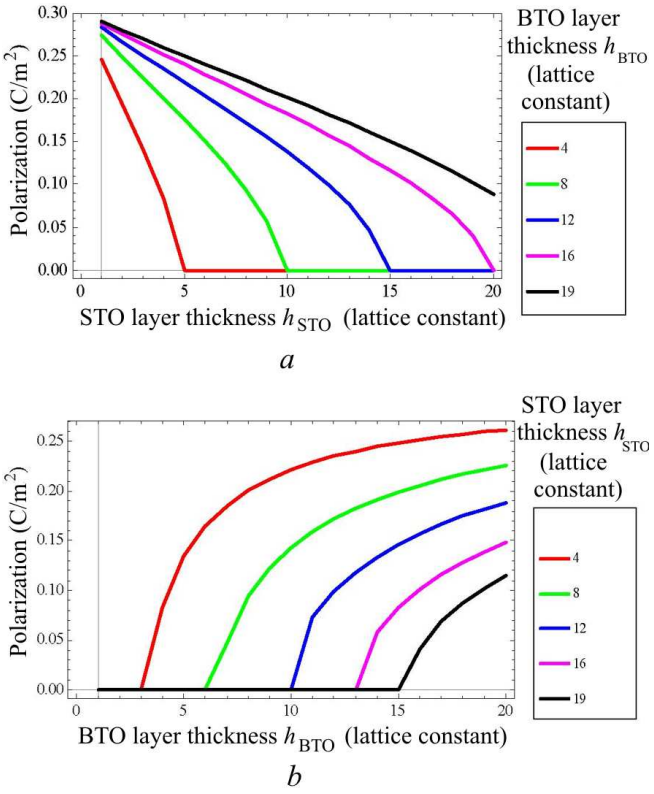

Fig. 4. (a) Dependences of the spontaneous polarization on the thickness h_{STO} of the virtual ferroelectric STO layer for various thicknesses h_{BTO} of the ferroelectric BTO layer. (b) Dependences of the spontaneous polarization on the thickness h_{BTO} of the ferroelectric BTO layer for various thicknesses h_{STO} of the virtual ferroelectric STO layer. Both parameters are expressed in units of lattice constant. The interface parameter $\gamma_3 = \gamma_i = 10^5$ C^{-2}m^{3}N, the misfit strain $u_m = -0.01$, the room temperature. Material parameters correspond to those of the multilayer BTO/STO film

a dielectric layer: the thicker the layer, the stronger is the depolarization field, which, in its turn, reduces the spontaneous polarization of the BTO film. On the other hand, the spontaneous polarization grows with the BTO film thickness (cf. different curves).

The dependences of the spontaneous polarization on the BTO ferroelectric layer thickness for various thicknesses of the STO film are shown in Fig. 4,*b*. One can see that the spontaneous polarization monotonously increases with the BTO film thickness and saturates tending to a bulk value of 0.26 C/m^2 inherent to the thinnest STO film. Therefore, the thicker the BTO layer, the stronger are its ferroelectric properties. On the other hand, the spontaneous polarization decreases with the increase of the STO film thickness, because the depolarization field grows (cf. different curves).

5. Calculation of Multilayer-Film Phase Diagram

To calculate the phase boundaries analytically, the linear dielectric susceptibility must be determined. The singularity in this parameter corresponds to the boundary between the para- and ferroelectric BTO phases. The linear dielectric susceptibility is determined from the linearized solution of Eq. (9) as $\chi_{ij}^{(i)} = \frac{dP_i^{(i)}}{dE_j^e}\Big|_{E_j^e \to 0}$. The results obtained are presented below.

5.1. Boundary between ferroelectric aa-phase and paraelectric phase

The polarization components in the aa-phase are $P_3^{(i)} = 0$ and $P_1^{(i)} = P_2^{(i)} \neq 0$. The boundary between the aa- and paraelectric phases in the $\left\{u_m^{(i)}, h_1, h_2, T\right\}$-coordinates is determined from the equations

$$0 = \left(\alpha_{S1}^{(1)} + \frac{g_{44}^{(1)}}{l_c^{(1)}} \tanh\left(\frac{h_1}{2l_c^{(1)}}\right)\right)\left(\alpha_{S1}^{(2)} + \frac{g_{44}^{(2)}}{l_c^{(2)}} \tanh\left(\frac{h_2}{2l_c^{(2)}}\right)\right) + \\ + \gamma_1 \left(\alpha_{S1}^{(1)} + \frac{g_{44}^{(1)}}{l_c^{(1)}} \tanh\left(\frac{h_1}{2l_c^{(1)}}\right) + \alpha_{S1}^{(2)} + \frac{g_{44}^{(2)}}{l_c^{(2)}} \tanh\left(\frac{h_2}{2l_c^{(2)}}\right)\right). \tag{10a}$$

Here, the transverse correlation length $l_c^{(i)} = \sqrt{g_{44}^{(i)}/a_1^{(i)}}$ is introduced, and it is supposed that $a_{1,2}^{(1)} > 0$. In the case where $a_1^{(1)} > 0$ and $a_1^{(2)} < 0$, it is necessary to redefine the correlation radius, $\tilde{l}_c^{(2)} = \sqrt{-g_{44}^{(2)}/a_1^{(2)}}$, and rewrite Eq. (10a) as follows:

$$0 = \left(\alpha_{S1}^{(2)} - \frac{g_{44}^{(2)}}{\tilde{l}_c^{(2)}} \tan\left(\frac{h_2}{2\tilde{l}_c^{(2)}}\right)\right) \times \\ \times \left(1 + \frac{\gamma_1}{\alpha_{S1}^{(1)} + \frac{g_{44}^{(1)}}{l_c^{(1)}} \tanh\left(\frac{h_1}{2l_c^{(1)}}\right)}\right) + \gamma_1 . \tag{10b}$$

In accordance with Eq. (3), Eqs. (10) depend on the misfit strain $u_m^{(i)}$ and the temperature T through the parameter $a_1^{(i)}$. We also put $\gamma_1^{(i-1)} = \gamma_1^{(i)} \equiv \gamma_1$. Note that the coefficients in Eqs. (10) depend not only on the misfit strain $u_m^{(i)}$ and the temperature T, but also on the layer thicknesses h_i. In fact, those equations determine the law of divergence for the denominator in the susceptibility $\chi_{11}^{(2)} = \frac{dP_1^{(2)}}{dE_1^e}\Big|_{E_1^e \to 0}$.

5.2. Boundary between the ferroelectric c-phase and the paraelectric phase

In the c-phase, the polarization components are $P_3^{(i)} \neq 0$ and $P_1^{(i)} = P_2^{(i)} = 0$. The boundary between the c-phase and the paraelectric phase in the $\left\{u_m^{(i)}, h_1, h_2, T\right\}$-coordinates is determined from the equations

$$\left(\begin{array}{l} A_{(1)}\varepsilon_{(1)2}\varepsilon_{(2)} a_3^{(2)} h_2 + A_{(2)}\varepsilon_{(2)2}\varepsilon_{(1)} a_3^{(1)} h_1 + \\ + \dfrac{2g_{11}^{(1)}\varepsilon_{(2)2}A_{(2)}\left(\gamma_3\left(\alpha_{S3}^{(2)}L_c^{(2)} + g_{11}^{(2)}\right) + \alpha_{S3}^{(1)}\left(g_{11}^{(2)} + L_c^{(2)}\left(\alpha_{S3}^{(2)} + \gamma_3\right)\right)\right) - 2\gamma_3 g_{11}^{(1)} g_{11}^{(2)} \varepsilon_{(1)}\varepsilon_{(2)} A_{(1)}}{A_{(1)}\left(\alpha_{S3}^{(1)}L_c^{(1)} + g_{11}^{(1)}\right)\left(\alpha_{S3}^{(2)}L_c^{(2)} + g_{11}^{(2)}\right) + \gamma_3\left(L_c^{(1)}L_c^{(2)}\left(\alpha_{S3}^{(1)} + \alpha_{S3}^{(2)}\right) + L_c^{(2)}g_{11}^{(1)} + L_c^{(1)}g_{11}^{(2)}\right)} + \\ + \dfrac{2g_{11}^{(2)}\varepsilon_{(1)2}A_{(1)}\left(\gamma_3\left(\alpha_{S3}^{(1)}L_c^{(1)} + g_{11}^{(1)}\right) + \alpha_{S3}^{(2)}\left(g_{11}^{(1)} + L_c^{(1)}\left(\alpha_{S3}^{(1)} + \gamma_3\right)\right)\right) - 2\gamma_3 g_{11}^{(1)} g_{11}^{(2)} \varepsilon_{(1)}\varepsilon_{(2)} A_{(2)}}{A_{(2)}\left(\alpha_{S3}^{(1)}L_c^{(1)} + g_{11}^{(1)}\right)\left(\alpha_{S3}^{(2)}L_c^{(2)} + g_{11}^{(2)}\right) + \gamma_3\left(L_c^{(1)}L_c^{(2)}\left(\alpha_{S3}^{(1)} + \alpha_{S3}^{(2)}\right) + L_c^{(2)}g_{11}^{(1)} + L_c^{(1)}g_{11}^{(2)}\right)} \end{array} \right) = 0, \tag{11}$$

where $\varepsilon_{(i)} = \varepsilon_0\varepsilon_b^{(i)}$, $A_{(i)} = a_3^{(i)} + \frac{1}{\varepsilon_{(i)}} \approx \frac{1}{\varepsilon_{(i)}}$, the longitudinal correlation length $L_c^{(i)} = \sqrt{g_{11}^{(i)}/A^{(i)}}$ $(i = 1, 2)$ is introduced, and the equalities $\gamma_3^{(i-1)} = \gamma_3^{(i)} \equiv \gamma_3$ are adopted. In fact, Eqs. (11) determine the divergence character of the denominator in the susceptibility $\chi_{33}^{(2)} = \frac{dP_3^{(2)}}{dE_3^e}\Big|_{E_1^e \to 0}$.

In the approximation $A_{(i)} \approx \frac{1}{\varepsilon_{(i)}}$ obtained from Eq. (11), we arrive at

$$a_3^{(2)}h_2 + a_3^{(1)}h_1 + \\ + 2\frac{\left(\begin{array}{l} g_{11}^{(1)}\left(\alpha_{S3}^{(1)}\left(L_c^{(2)}\alpha_{S3}^{(2)} + g_{11}^{(2)}\right) + \gamma_3 L_c^{(2)}\left(\alpha_{S3}^{(2)} + \alpha_{S3}^{(1)}\right)\right) + \\ + g_{11}^{(2)}\left(\alpha_{S3}^{(2)}\left(L_c^{(1)}\alpha_{S3}^{(1)} + g_{11}^{(1)}\right) + \gamma_3 L_c^{(1)}\left(\alpha_{S3}^{(2)} + \alpha_{S3}^{(1)}\right)\right) + \gamma_3 g_{11}^{(1)} g_{11}^{(2)}\left(\varepsilon_0\varepsilon_b^{(1)}a_3^{(1)} - \varepsilon_0\varepsilon_b^{(2)}a_3^{(2)}\right)^2 \end{array} \right)}{\left(\alpha_{S3}^{(1)}L_c^{(1)} + g_{11}^{(1)}\right)\left(\alpha_{S3}^{(2)}L_c^{(2)} + g_{11}^{(2)}\right) + \gamma_3\left(L_c^{(1)}L_c^{(2)}\left(\alpha_{S3}^{(1)} + \alpha_{S3}^{(2)}\right) + L_c^{(2)}g_{11}^{(1)} + L_c^{(1)}g_{11}^{(2)}\right)} \approx 0. \tag{12}$$

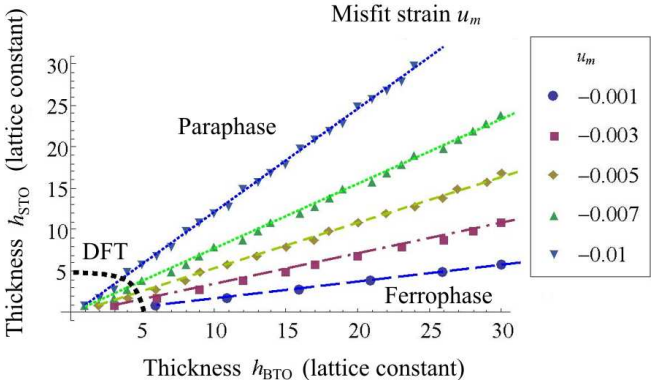

Fig. 5. Phase diagrams of a multilayer BTO/STO structure in the coordinates $\{h_{\rm BTO}, h_{\rm STO}\}$ at room temperature and various misfit strains u_m. $\gamma = 10^5$ C^{-2}m^{3}N and $\alpha_{Sj}^{(i)} = 0$. Every straight line is a corresponding boundary between the para- (above) and ferroelectric (below) phases

In Fig. 5, the phase diagrams of multilayer structures, which can be either in the ferroelectric (polar) phase or in the paraelectric (nonpolar) one, are shown as functions of the thicknesses of their STO and BTO films.

The dashed line bounds the region, where the thicknesses of both films are smaller than 5 lattice constants. Here, the coefficients of the free energy expansion in the framework of a phenomenological theory are unknown, because it cannot be applied owing to quantum-size effects. On such scales, the methods of density functional theory have to be used in calculations.

The boundaries between the BTO ferroelectric phases in the $\left\{u_m^{(i)}, h_1, h_2, T\right\}$-coordinates were calculated numerically.

5.3. *Phase diagram of multilayer $SrTiO_3/BaTiO_3$ films*

The phase diagrams for a thin BTO film and multilayer $SrTiO_3/BaTiO_3$ films are shown in Fig. 6. As one can see, the boundaries between the paraelectric (PE) and ferroelectric (FE) phases are straight lines.

It turned out that there can exist six thermodynamically stable phases in multilayered $SrTiO_3/BaTiO_3$ films–one paraelectric phase and five ferroelectric ones: a tetragonal (FEc), two monoclinic (FEaac and FEac), and two orthorhombic (FEa and FEaa) phases. Such a situation takes place in contrast to bulk $BaTiO_3$, for which only four phases (paraelectric, tetragonal, orthorhombic, and rhombohedral) exist [22].

Qualitatively, the phase diagrams of thin BTO and multilayer $SrTiO_3/BaTiO_3$ films are similar. The quantitative difference consists in that the range of the paraelectric phase extends with the increase of the $SrTiO_3$ layer thickness, because $SrTiO_3$ plays the role of a dielectric layer: the thicker the layer, the stronger is the depolarization field, which, in its turn, reduces the spontaneous polarization of the $BaTiO_3$ film. Simultaneously, the regions of the FEc ($P_3^{(i)} \neq 0$ and $P_1^{(i)} = P_2^{(i)} = 0$) and FEaac ($P_3^{(i)} \neq 0$ and $P_1^{(i)} = P_2^{(i)} \neq 0$) phases decrease, being governed by the same mechanism. The phase boundaries change their shapes, as the thickness of $SrTiO_3$ layers increases. It is evident that the existence range for the PE phase is minimal for a thin film, whereas, for multilayer films, it is larger for thicker STO layers. STO plays the role of a dielectric interlayer, which weakens the ferroelectric properties of a multilayer film. The boundary of the PE phase with other phases looks like a straight line. The total area of FE regions, where $P_3^{(i)} \neq 0$, decreases with the increase of the STO layer thickness. In other words, it is beneficial for multilayer films with thick STO layers to be polarized in the film plane. Every phase diagram depicted in Fig. 6 includes six thermodynamically stable $BaTiO_3$ phases.

6. Conclusions

The main polar properties of hysteresis loops (shape, coercive field, and spontaneous polarization) for thin multilayer films have been calculated. It was shown that, in the system concerned, there exists a strong dependence of their polar properties on the thickness of SrTiO and BaTiO layers. In particular,

1) the coercive field monotonously grows with the BTO film thickness; on the other hand, it decreases as the thickness of the $SrTiO_3$ film grows, and, as a result, the depolarization electric field increases;

2) the spontaneous polarization monotonously decreases as the $SrTiO_3$ film thickness grows, so that $SrTiO_3$ plays the role of a dielectric layer: the thicker the layer, the stronger is the depolarization field, which, in its turn, reduces the spontaneous polarization of the $BaTiO_3$ film; on the other hand, the spontaneous polarization grows with the $BaTiO_3$ film thickness;

3) the spontaneous polarization firstly monotonically increases with the BTO film thickness and then saturates, by approaching a bulk value of 0.26 C/m^2 inherent to

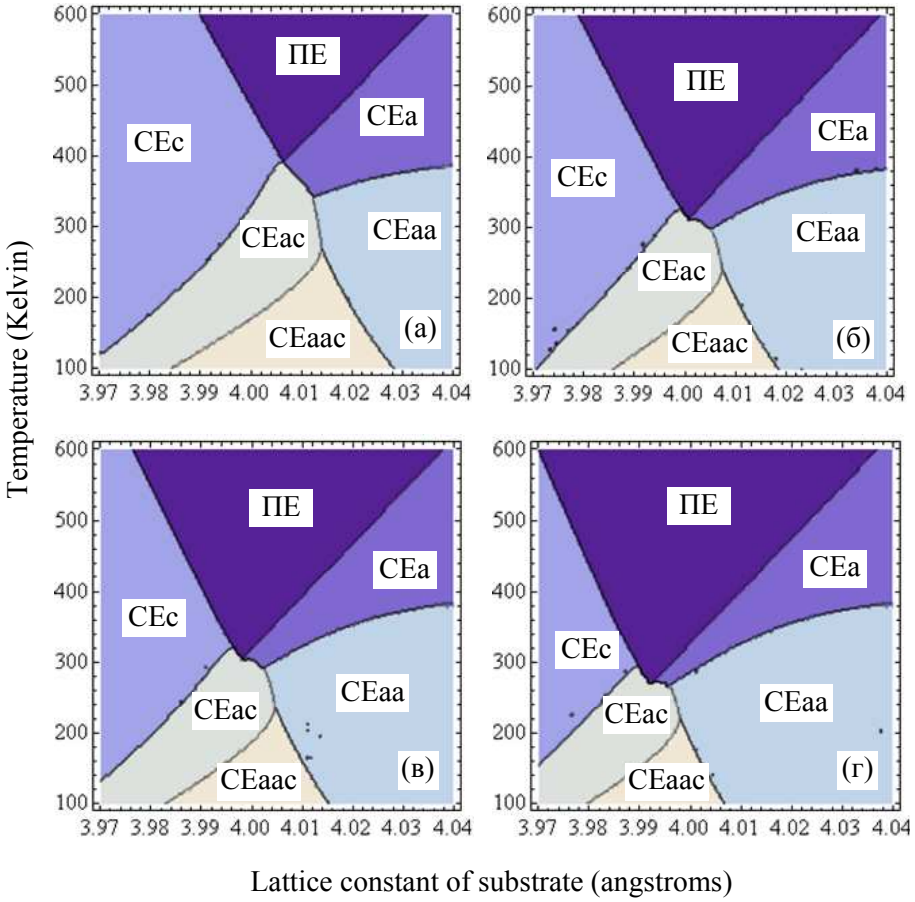

Fig. 6. Phase diagrams in the coordinates "substrate lattice constant versus the temperature" for (*a*) thin BTO film and (*b*–*d*) multilayer films consisting of 8-nm BTO layers and STO layers 0.8 (*b*), 1.2 (*c*), and 2.4 nm (*d*) in thickness (the layers repeat periodically). The parameters of the phases are as follows. PE phase: $P_3^{(i)} = P_1^{(i)} = P_2^{(i)} = 0$; FEc phase: $P_3^{(i)} \neq 0$ and $P_1^{(i)} = P_2^{(i)} = 0$; FEa phase: $P_3^{(i)} = P_2^{(i)} = 0$ and $P_1^{(i)} \neq 0$; FEaa phase: $P_3^{(i)} = 0$ and $P_1^{(i)} = P_2^{(i)} \neq 0$; FEac phase: $P_3^{(i)} \neq 0$, $P_1^{(i)} = 0$, and $P_2^{(i)} \neq 0$; and FEaac phase: $P_3^{(i)} \neq 0$ and $P_1^{(i)} = P_2^{(i)} \neq 0$. The interface parameter $\gamma_3 = \gamma_i = 10$ $C^{-2}m^3N$ and $\alpha_{Sj}^{(i)} = 0$. The parameter values were taken from work [23]

a thin $SrTiO_3$ film; the thicker the $BaTiO_3$ layer, the stronger are its ferroelectric properties; on the other hand, the spontaneous polarization decreases with the growth of the $SrTiO_3$ film thickness, owing to the growth of the depolarization field;

4) the thickness of the BTO layer, at which the system transforms into the ferroelectric phase, linearly grows with the STO layer thickness;

5) it turned out that six thermodynamically stable $BaTiO_3$ phases – one paraelectric and five ferroelectric (tetragonal FEc, two monoclinic FEaac and FEac, and two orthorhombic FEa and FEaa) – can exist in multilayer $SrTiO_3/BaTiO_3$ films, in contrast to bulk $BaTiO_3$, where only four phases exist (paraelectric, tetragonal, orthorhombic, and rhombohedral ones).

APPENDIX

T a b l e 1. Free energy parameters for bulk ferroelectric $BaTiO_3$

Landau parameters for free energy	Value	Parameters for elastic energy	Value
α_1 ($10^5 C^{-2}\cdot m^2\cdot N$)	3.61(T–391)	$s_{11}(C^{-12}\cdot m^2/N)$	8.3
$\alpha_{11}(10^9\ C^{-4}\cdot m^6\cdot N)$	–1.83	$s_{12}(C^{-12}\cdot m^2/N)$	–2.7
$\alpha_{12}(10^9\ C^{-4}\cdot m^6\cdot N)$	–2.24	$s_{44}(C^{-12}\cdot m^2/N)$	9.24
$\alpha_{111}(10^{10}\ C^{-6}\cdot m^{10}\cdot N)$	1.39	Parameters for gradient energy	Value
$\alpha_{112}(10^9\ C^{-6}\cdot m^{10}\cdot N)$	–2.2	$g_{11}(10^{-10}C^{-2}\cdot m^4\cdot N)$	2.0
$\alpha_{123}(10^{10}\ C^{-6}\cdot m^{10}\cdot N)$	5.51	$g_{44}(10^{-10}C^{-2}\cdot m^4\cdot N)$	1.0
$Q_{11}(C^{-2}\cdot m^4)$	0.11		
$Q_{12}(C^{-2}\cdot m^4)$	–0.043	$G_{110}(10^{-10}C^{-2}\cdot m^4\cdot N)$	1.73
$Q_{44}(C^{-2}\cdot m^4)$	0.059		

T a b l e 2. Free energy parameters for bulk virtual ferroelectric $SrTiO_3$

Parameter	Measurement units	Virtual ferroelectric	
		$SrTiO_3$	Reference
Background permittivity ε_b	dimensionless	3–43	[24]
Coefficient α_T in LGD expansion	10^6 m/(F·C)	1.66	[25, 26]
Curie temperature T_0	K	36	[25, 26]
Temperature of quantum-mechanical vibrations T_q	K	100	[25, 26]
LGD gradient coefficient g	10^{-10} B·m^3/C	1–5	[27]
Coefficients α_{ij} in LGD expansion	10^9 m^5/(C^2·F)	$\alpha_{11} = 8.1$ $\alpha_{12} = 2.4$	[25, 26]
Coefficients α_{ijk} in LGD expansion	10^{12} m^9/(C^4·F)	~ 1	Undefined
Electrostriction coefficients Q_{ijkl}	m^4/C^2	$Q_{11} = 0.051$ $Q_{12} = -0.016$ $Q_{44} = 0.020$	[28]
Elastic rigidity c_{ij}	10^{11} N/m^2	$c_{11} = 3.36$ $c_{12} = 1.07$ $c_{44} = 1.27$	[28]
Elastic compliance s_{ij}	10^{-12} m^2/N	$s_{11} = 3,89$ $s_{12} = -1.06$ $s_{44} = 8.20$	[28]

1. R. Nath, S. Zhong, S.P. Alpay, B.D. Huey, and M.W. Cole, Appl. Phys. Lett. **92**, 012916 (2008).
2. J.Y. Jo, R.J. Sichel, E.M. Dufresne, H.N. Lee, S.M. Nakhmanson, and P.G. Evans, Phys. Rev. B **82**, 174116 (2010).
3. J.Y. Jo, R.J. Sichel, H.N. Lee, S.M. Nakhmanson, E.M. Dufresne, and P.G. Evans, Phys. Rev. Lett. **104**, 207601 (2010).
4. V.A. Stephanovich, I.A. Luk'yanchuk, and M.G. Karkut, Phys. Rev. Lett. **94**, 047601 (2005).
5. D.G. Schlom, L.-Q. Chen, X. Pan, A. Schmehl, and M.A. Zurbuchen, J. Am. Ceram. Soc. **91**, 2429 (2008).
6. X. Wu, K.M. Rabe, and D. Vanderbilt, Phys. Rev. B **83**, 020104 (2011).
7. A.L. Roytburd, S. Zhong, and S.P. Alpay, Appl. Phys. Lett. **87**, 092902 (2005).
8. E. Bousquet, M. Dawber, N. Stucki, C. Lichtensteiger, P. Hermet, S. Gariglio, J.-M. Triscone, and P. Ghosez, Nature **452**, 732 (2008).
9. D.D. Fong, G.B. Stephenson, S.K. Streiffer, J.A. Eastman, O. Auciello, P.H. Fuoss, and C. Thompson, Science **304**, 1650 (2004).
10. M.B. Okatan, J.V. Mantese, and S.P. Alpay, Acta Mater. **58**, 39 (2010).
11. M.B. Okatan, I.B. Misirlioglu, and S.P. Alpay, Phys. Rev. B **82**, 094115 (2010).
12. I.B. Misirlioglu, G. Akcay, and S. Zhong, J. Appl. Phys. **101**, 036107 (2007).
13. N.A. Pertsev, V.G. Kukhar, H. Kohlstedt, and R. Waser, Phys. Rev. B **67**, 054107 (2003).
14. A. Sharma, Z.-G. Ban, S.P. Alpay, and J.V. Mantese, J. Appl. Phys. **95**, 3618 (2004).
15. Z.-G. Ban and S. P. Alpay, Appl. Phys. Lett. **82**, 3499 (2003).
16. B.D. Qu, W.L. Zhong, and R.H. Prince, Phys. Rev. B **55**, 11218 (1997).
17. K.H. Chew, Y. Ishibashi, and F.G. Shin, Ferroelect. **357**, 133 (2007).
18. N.A. Pertsev, A.G. Zembilgotov, and A.K. Tagantsev, Phys. Rev. Lett. **80**, 1988 (1998).
19. J.S. Speck and W. Pompe, J Appl. Phys. **76**, 466 (1994).
20. G. Rupprecht and R.O. Bell, Phys. Rev. A **135**, 748 (1964).
21. C.-L. Jia, V. Nagarajan, J.-Q. He, L. Houben, T. Zhao, R. Ramesh, K. Urban, and R. Waser, Nature Mater. **6**, 64 (2007).
22. G.A. Smolenskii, V.A. Bokov, V.A. Isupov, N.N. Krainik, R.E. Pasynkov, and A.I. Sokolov, *Ferroelectrics and Related Materials* (Gordon and Breach, New York, 1984).
23. Y.L. Wang, A.K. Tagantsev, D. Damjanovic, N. Setter, V.K. Yarmarkin, and A.I. Sokolov, J. Appl. Phys. **101**, 104115 (2007).
24. A. Fleury and J.M. Worlock, Phys. Rev. **174**, 613 (1968).
25. H. Uwe and T. Sakudo, Phys. Rev. B **15**, 337 (1977).
26. The order of magnitude $g \sim 10^{-10}$ V $\cdot$ m^3/K corresponds to ordinary "rigid" ferroelectrics like PTO, whereas $g \sim 10^{-9}$ V $\cdot$ m^3/K seems to be more typical of virtual ferroelectrics, "soft" ferroelectrics, and ferroelectric semiconductors.
27. A. Pertsev, A.K. Tagantsev, and N. Setter, Phys. Rev. B **61**, 825 (2000).

Received 01.09.11.
Translated from Ukrainian by O.I. Voitenko

ПОЛЯРНІ ВЛАСТИВОСТІ ТА ПЕТЛІ ГІСТЕРЕЗИСУ У БАГАТОШАРОВИХ ТОНКИХ ПЛІВКАХ ТИПУ СЕГНЕТОЕЛЕКТРИК/ВІРТУАЛЬНИЙ СЕГНЕТОЕЛЕКТРИК

Є.А. Єлісєєв, М.Д. Глинчук, Г.М. Морозовська, Я.В. Яковенко

Р е з ю м е

Використовуючи феноменологічну теорію Ландау–Гінзбурга–Девоншира, розраховано вплив деформацій невідповідності, поверхневої енергії та розмірних ефектів на фазові діаграми, полярні властивості та петлі гістерезису у багатошарових тонких плівках типу сегнетоелектрик/віртуальний сегнетоелектрик. Вперше досліджено вплив пружних деформацій, що виникають на межі тонка плівка–підкладка внаслідок невідповідності сталих ґратки плівки та підкладки, на фазові діаграми багатошарових тонких плівок складу віртуальний сегнетоелектрик $SrTiO_3$/сегнетоелектрик $BaTiO_3$. Виявилося, що у багатошарових плівках складу $SrTiO_3/BaTiO_3$ можуть існувати шість термодинамічно стійких фаз $BaTiO_3$ (параелектрична, тетрагональна FEc, дві моноклінні: FEaac та FEac, дві орторомбічні: FEa та FEaa сегнетоелектричні фази) на відміну від об'ємного $BaTiO_3$, де існують лише чотири фази (кубічна, тетрагональна, орторомбічна та ромбоедрична). Розраховано основні полярні властивості петель гістерезису (форма, коерцитивне поле і спонтанна поляризація) у тонких багатошарових плівках $SrTiO_3/BaTiO_3$. Показано, що у системі існує сильна залежність полярних властивостей від товщини шарів $SrTiO_3$ і $BaTiO_3$ та пружних деформацій невідповідності, причому $SrTiO_3$ відіграє роль діелектричного прошарку: чим товщий прошарок, тим сильніше поле деполяризації, яке, у свою чергу, зменшує спонтанну поляризацію плівки $BaTiO_3$.